Chapter 6 - Categorization of soft objects during haptic exploration tasks

Google Scholar and other services only track the citations of the full version of the PhD thesis.

Chapter 6

Categorization of soft objects during haptic exploration tasks

6.1 Introduction

Due to the introduction of robotic platforms in new types of environments (chapter 1), the principles and demands guiding the implementation of robotic platforms are changing. The robotic systems need to interact autonomously with a wide variety of objects (size, shape, compliance, and texture) [Feix et al., 2014]. The work presented in this chapter is focused on the study of objects with different hardness-softness properties [Tiest, 2010].

Typically, the autonomous planning of a robotic manipulation task starts by the estimation of an initial model of the object, through the extraction of features from the vision data, as described in chapter 2 and [Bohg, 2011]. The initial estimation of distance to object, shape affordances, and other characteristics of the surface is based on previous perceptual experiences. It allows the robot to infer several parameters of the reach-to-grasp movement and initial grasp required to hold the object without slipping.

The contributions presented in this chapter are associated with the manipulation movements happening after this initial interaction. When the perceived model representing the object is not sufficiently informative to perform the required task, the system uses the robotic hand to explore the object progressively. The haptic exploration movements are used to perceive complementary properties of the object such as hardness, texture, weight, shape, and temperature (chapter 3).

This chapter presents a probabilistic spatial framework suitable to integrate multi-modal data (vision, tactile, and motion) acquired during the interaction with an object. The multi-modal data is used to build a perceptual model of the manipulated object and infer the category of material being explored. The categories of material considered in this chapter have different perceived hardness characteristics. In terms of hardness characteristics, this work considers the perception that the robotic hand receives when it interacts with objects made of compliant materials. The methods proposed in this

chapter do not achieve a full, precise, and universal characterization of the objects as studied in materials science (stiffness, Young's modulus, mass spring system, finite element methods). The approach presented in this chapter formulates a descriptor defined from features extracted during the interaction between an exploratory element and a surface, to discriminate different objects using its previous knowledge about a finite set of objects.

The description of the perceived hardness can contribute to the discrimination and recognition of objects and adapt the manipulation strategies accordingly.

6.2   Related works

The study of deformable objects has been a research field explored extensively in very different areas: computer vision [Dufour et al., 2011] (tracking, reconstruction, and recognition), computer graphics [Garre et al., 2011] [Ni et al., 2011] (primarily for rendering purposes), industrial materials sciences (very restricted and controlled tests and applications labs or clean rooms with high-accuracy measurement devices), medicine [Liu et al., 2010a] [Ni et al., 2011] (organ analysis and anatomical abnormality detection, virtual haptics simulation for medical training).

Table 6.1: Comparison between the contributions of this work and the related works

Study	Apparatus		Haptic Perception	
	Platform [a]	Sensing [b]	Approach [c]	Features [d]
This work	HH	HS	P	CI, CD
[Okamura et al., 2001]	RS	HS	D	C
[Oddo et al., 2011]	RS	HS	D	V, T
[Hongbin Liu, 2011]	RS	HS	P	F
[Fishel and Loeb, 2012]	RS	HS	P	CD, CI, V, H
[Hui and Kuchenbecker, 2014]	RS	HS	D	CI, CD
[Xu et al., 2013]	RS	HS	P	CI, V, T
[Faria et al., 2012]	HH	HS, VS	P	C, L
[Chitta et al., 2011]	RS	HS	D	CI
[Frank et al., 2010]	RS	HS, VS	D	L, CI, CD

[a] RS- robotic system; HH- human hand.
[b] HS- haptic sensing; VS- visual sensing.
[c] P- probabilistic; D- deterministic.
[d] T- texture; C- curvature; F- friction coefficient; L- RGBD cloud points; CI- contact intensity; CD-contact indentation; V- micro-vibration; H- heat flow.

Typically, soft objects can be represented by 3D computational models in the discrete (e.g. mass spring systems) or continuous (e.g. finite element methods) domain. This type of computational model provides an accurate description of the dynamics of soft objects. However, the elaboration of this type of model by an autonomous robotic platform faces several challenges and constraints.

Some experimental conditions of the material sciences laboratories are difficult to replicate in the context of autonomous robotic manipulation (restrictions on hardware design: hand dexterity, calibration accuracy of tactile and vision sensors, real-time computational

power, and energy efficiency). Additionally, autonomous robotic platforms must deal with the uncertainty associated with the dynamics of the environment and noise of the data measurements.

In the cognitive autonomous robotic manipulation field, different approaches have been proposed to improve the perceived representation of the object during the manipulation and exploration tasks. Some approaches are dedicated to the estimation of the surface characteristics of the object, such as texture and stickiness. [Hongbin Liu, 2011] proposes an algorithm to categorize objects using the surface friction properties. The friction coefficients of the surfaces are estimated from force and torque data sensed by a robotic finger.

The work by [Oddo et al., 2011] proposes the design of a robotic fingertip with an artificial haptic perception system for surface texture discrimination. [Okamura et al., 2001] proposes a method to identify different types (cusp, step, and bump) of surface features during the lateral sliding of a robotic finger.

Recently, several works have used the *Biotac* robotic fingertip to discriminate objects. This compact device replicates the anatomic characteristics of a human fingertip, being capable of sensing temperature, micro-vibration, and pressure. [Fishel and Loeb, 2012] applied lateral sliding movements of a metallic bar equipped with *Biotac* to recognize different textures. The work also studied the impact of velocity and pressure of lateral sliding movement to the performance of the system. The work by [Hui and Kuchenbecker, 2014] used the *Biotac* device integrated on the tip of a probe to explore simulated samples of tissues. Haptic palpation was used to recognize lumps on tissues by integrating pressure and indentation depth features. The work of [Xu et al., 2013] integrates *Biotac* fingertip on a *Shadow* robotic hand and performs two types of exploratory movements to extract three type of haptic features: texture (lateral sliding movement), compliance (palpation/press-and-release), and heat flow (palpation/press-and-release). These three features are integrated simultaneously to discriminate different classes of objects.

Other works are focused on representing the perceived shape of the object to find suitable regions for stable grasping. [Faria et al., 2012] builds a volumetric representation of the shape of the object as long as the object is progressively explored. The representation is decomposed in volumetric primitives, and the best elementary regions for stable grasping are identified based on human demonstrations. [Chitta et al., 2011] infers the internal state (empty, full, open, closed) and recognizes objects using deformation signatures during a haptic exploration task. The approach only uses tactile data.

The work of [Frank et al., 2010] tries to integrate information from a vision and force/torque sensing system to estimate the elasticity properties of objects during a haptic exploration task. The work establishes a relation between the deformation induced by the

robotic end-effector and the intensities of the sensed forces. Different objects have distinct deformation / force intensity signatures. The work does not use a dexterous robotic hand to interact with the object. A rectangular bar is used to explore the environment.

The motivation for this work is introduced in section 6.1. The proposed approach is summarized in section 6.3 and compared with related works in Table 6.1.
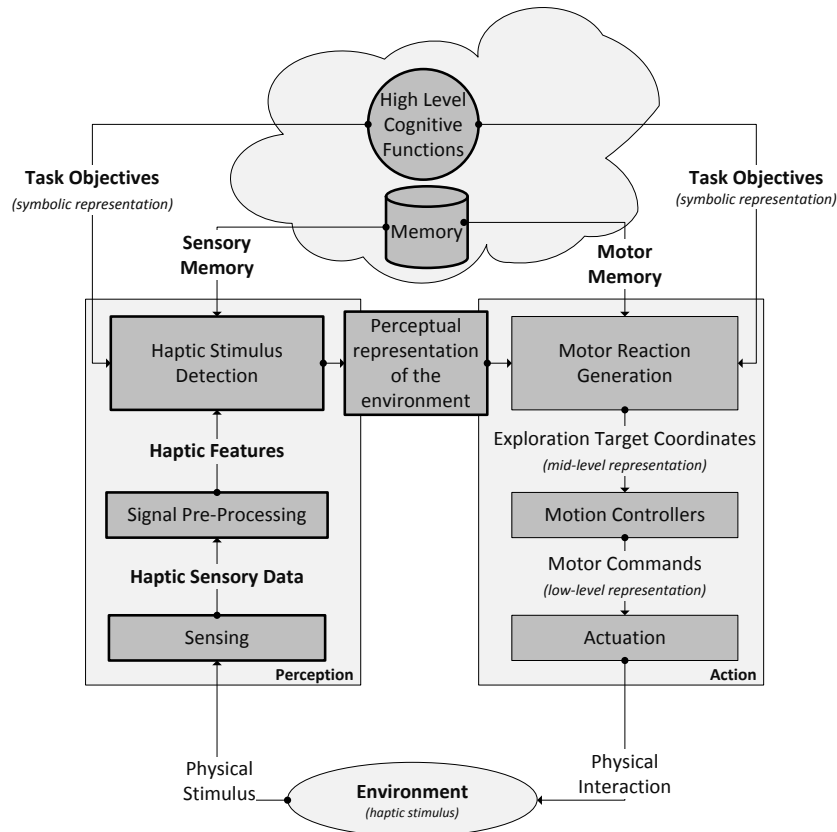

Figure 6.1: Schematic representation of the action-perception loop involved in the haptic exploration of surfaces. The elements highlighted with bold border are discussed in this chapter.

6.3   Approach overview

To endow the robotic systems with the capability to recognize and categorize distinct materials (different hardness-softness properties), the approach presented in this chapter analyses the principles and strategies used by humans to perform such types of tasks. The capability to discriminate the materials results from the integration of different types of haptic data.

During the haptic exploration tasks, the perception and discrimination of hardness-
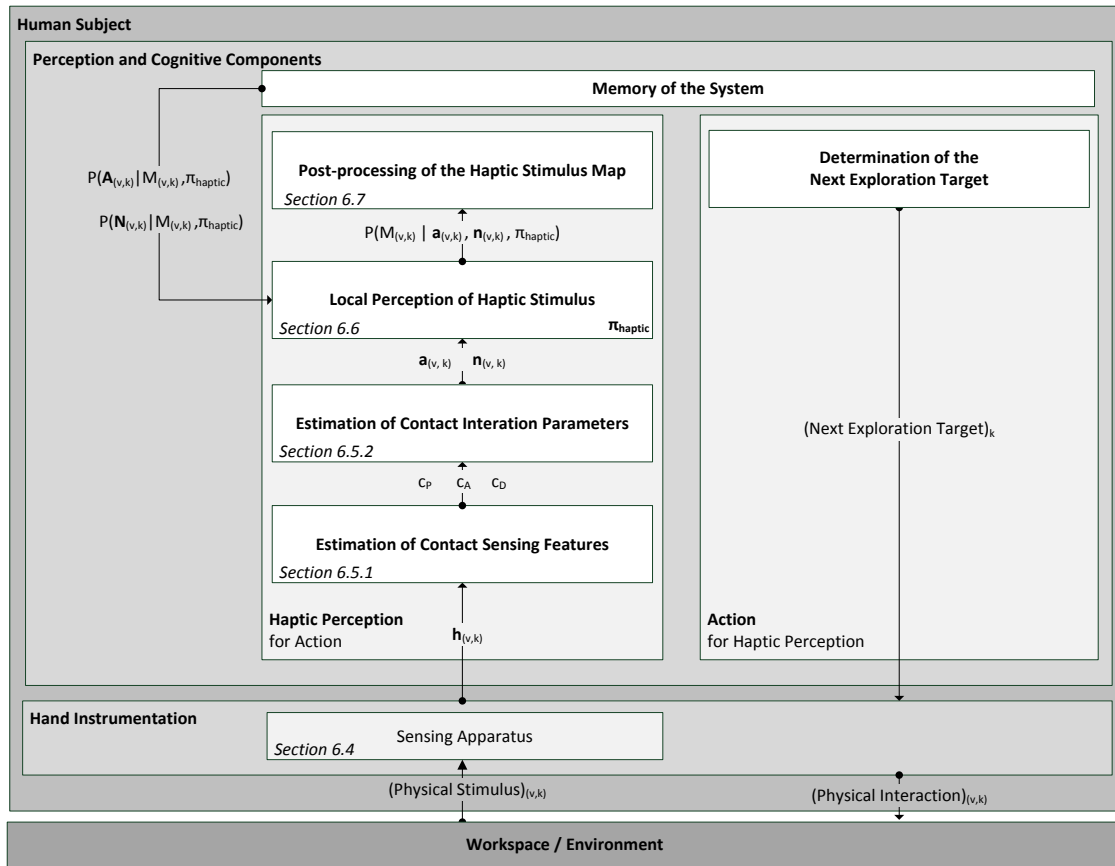
Figure 6.2: Global architecture of the approach presented in this chapter. The main contributions are identified and referenced in the scheme (description of the sensing apparatus, estimation of the contact interaction parameters, local perception of haptic stimulus, and post-processing of haptic stimulus map). The variables involved in the flow of data are summarized in Table 6.2.

Table 6.2: Summary of the relevant variables used in this chapter

Variable	Description	Domain
v	Cell of the workspace grid.	$\mathbb{R}^2$
k	Time / exploration iteration.	$\mathbb{N}^0$
$\mathbf{h}_{(v,k)}$	Raw haptic sensing data acquired on v.	$\mathbb{R}^n$ *
c_P	Contact sensing: intensity.	$\mathbb{R}_0^+$
c_A	Contact sensing: area.	$\mathbb{R}_0^+$
c_D	Contact sensing: indentation distance.	$\mathbb{R}_0^+$
$M_{(v,k)}$	Material category of v	$\{Material_1, \ldots, Material_3\}$
$A_{(v,k)}$	Cutaneous contact interaction parameters.	$\mathbb{R}^2$
$N_{(v,k)}$	Kinesthetic contact interaction parameters.	$\mathbb{R}^2$
$H(v)$	Entropy of the grid cell v.	$\mathbb{R}$

* In this work, the description of the sensory apparatus of the instrumented hand platform follows a generic formulation. In this context, n represents the dimensionality of the raw sensing data provided by the haptic sensory apparatus of the robot.

softness characteristics of objects depends on the simultaneous integration of cutaneous and kinesthetic information by performing "press-and-release" movements [Lederman and Klatzky, 1987] - active haptic perception. This haptic exploration strategy and integration of multi-modal data was demonstrated by psychophysical experiments performed in [Srinivasan and LaMotte, 1995] and [Lederman and Klatzky, 1987], respectively.

As described in detail in chapter 3 and shown using a simplified representation in Figure 6.1, several types of haptic features can be extracted from the cutaneous and kinesthetic data. In this chapter, the human hand is instrumented with a tactile sensing array and a motion tracking system, described in section 6.4.

The haptic data is subjected to a feature extraction processing pipeline formulated in chapters 6.5.1 (extraction of contact sensing features) and 6.5.2 (extraction of contact interaction parameters). The features extracted in the previous stages are integrated by the Bayesian model π_{haptic} "Local Perception of the Haptic Stimulus" (chapter 6.6).

The Bayesian model π_{haptic} infers and updates the category of material describing the region of the workspace which was explored. The workspace is represented by a planar 2D probabilistic (inference) grid (details about this representation framework are provided in chapter 2). The description of the perceived category of material is updated after each haptic exploration iteration step, integrating new sensory inputs on the haptic processing pipeline and on the Bayesian model π_{haptic}.

This representation framework is suitable to integrate noisy multi-modal sensory inputs from multiple exploratory elements (dexterous robotic hands). The grid also allows the representation of non-homogeneous objects/surfaces.

In this chapter, a exploration iteration step corresponds to a press-and-release exploration movement. This is the exploration pattern used to extract hardness-softness properties of objects (literature review presented in chapter 3). The perceived spatial representation of the object is improved and optimized using methods presented in section 6.7.

In the approach proposed in this chapter, the press-and-release movements are performed at pre-defined locations of the workspace. In the next chapter of this thesis (chapter 7), the the regions of the workspace which are going to be explored next are inferred online and autonomously as the exploration progresses (closes the action-perception loop).

6.4   Haptic sensory data

During the haptic exploration of an object, the sensory apparatus interacts with the object producing raw sensory outputs represented by the variable $\mathbf{h}_{(v,k)}$. The type of sensory
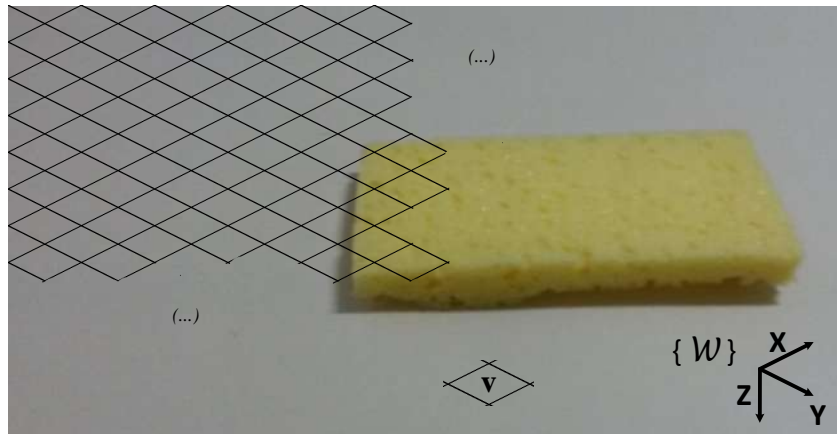
Figure 6.3: Partial representation of the bidimensional grid framework, which is used to describe the workspace region (e.g.: sponge object).

outputs $\mathbf{h}_{(v,k)}$ produced during the exploration process is dependent on the technology and design of the sensing apparatus (force, torque, tactile, temperature, vibration; single point, array), as well as the type of movement strategy used to perform the haptic exploration.

The methods proposed in this chapter are defined following a generic formulation. This work considers that the agent involved in the exploration process is equipped with a tactile sensing array and that the exploration strategy consists of a sequence of "press-and-release" (palpation) movements.

Thus, at each time iteration k, the haptic sensory output resulting from the interaction between the exploratory element and the material at the region v of the workspace is described by the variable presented in equation 6.1.

$$\mathbf{h}_{(v,k)} = (h^1, h^2, \ldots, h^N, h^X, h^Y, h^Z)$$
$$h^1, h^2, \ldots, h^N \in \mathbb{R}_0^+, \quad h^X, h^Y, h^Z \in \mathbb{R} \tag{6.1}$$

The variables $h^1, h^2, \ldots, h^N$, represent the tactile sensing outputs of each of the N elements of the tactile sensing array. The outputs h^i express the contact intensity sensed by each element of the array. The Cartesian coordinates of the end-effector of the exploration system are expressed in the inertial reference frame $\{\mathcal{W}\}$ and represented by the variables h^X, h^Y, h^Z.

A cell v of the bidimensional grid and the inertial reference frame $\{\mathcal{W}\}$ are illustrated in Figure 6.3.
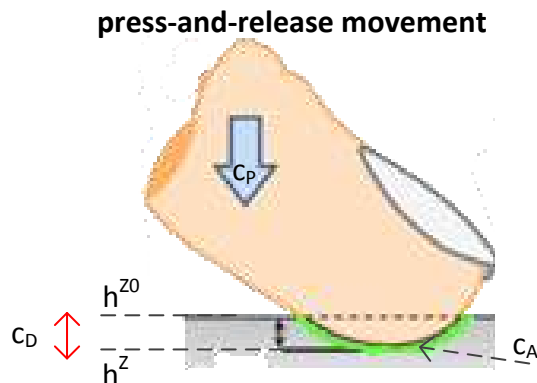
Figure 6.4: Schematic representation of the contact sensing variables extracted during the haptic exploration of a surface. Variables described in section 6.5. Image adapted from [van Kuilenburg et al., 2013].

6.5   Pre-processing of the haptic sensory data

6.5.1   Determination of the contact sensing features c_P, c_D, c_A

The sensory outputs $\mathbf{h}_{(v,k)}$ presented in equation 6.1 are processed to extract features modelling the contact interaction behaviour of the material. A description of the contact sensing features is presented in Figure 6.4.

The total intensity of the contact is described by the variable c_P presented in equation 6.2. This variable corresponds to the total sum of the individual outputs of the elements h^j of the tactile array.

$$c_P = \sum_{j=1}^{N} h^j \tag{6.2}$$

As long as the "press-and-release" exploration movement is performed, the area of the tactile sensing array contacting the surface of the object changes. This area is described by the variable c_A described in equation 6.3 .

$$c_A = \vartheta h^a$$
$$\vartheta = \#\{\forall_{h^j} : h^j > 0\}$$
$$c_A \in [0, N h^a] \tag{6.3}$$

The total area of contact interaction is determined by the number of active tactile sensing elements of the array, ϑ, and the area, h^a, of each element of the array, as described in equation 6.3. A sensing element of the tactile array is considered active if its individual output h^j is higher than zero (equation 6.3). This means that if a sensing elements is contacting the object, the sensing element is active.

In this work, the objects to be explored are made of soft materials. Thus, during a "press-and-release" exploration movement, the deformation of the surface of the object can be described by the variable c_D, as shown in equation 6.4 and illustrated in Figure 6.4.

$$c_D = h^Z - h^{Z_0}$$
$$c_D \in \mathbb{R}_0^+ \tag{6.4}$$

This work considers that the "press-and-release" exploration motion is performed uni-axially along the Z axis of the inertial reference $\{\mathcal{W}\}$. Considering this, c_D measures the indentation distance, h^Z, of the exploratory element relative to the point where it made the initial contact with the natural surface of the object, h^{Z_0}.

The contact sensing features c_A, c_P, c_D extracted from the haptic sensory data $\mathbf{h}_{(v,k)}$ are used as input to the estimation of the contact interaction parameters described in section 6.5.2.

6.5.2   Estimation of the cutaneous and kinesthetic interaction parameters

During a "press-and-release" exploration movement, several samples of the features c_A, c_P, c_D are acquired. The profile represented by the set of the corresponding data points (c_A, c_P, c_D) encodes relevant information about the haptic characteristics of the material being explored and can be used to discriminate different classes of materials.

The categorization of different materials based on their contact interaction signature can be performed by integrating two different sources of information. As demonstrated by [Scilingo, 2010], the simultaneous integration of information related to cutaneous tactile

sensing (relation between contact intensity and contact area) and information related to kinesthetic sensing (relation between contact intensity and contact indentation level) during a haptic exploration task, is essential to perceive and discriminate soft materials based on their haptic properties. This multi-modal integration is also essential to resolve some ambiguities which can occur if each of type of information is used separately.

Considering an exploratory element with a spherical design [Scilingo, 2010] (e.g.: human fingertip), the cutaneous component of the contact interaction signature is described by the relation presented in equation 6.5.

$$c_P = a_1 c_A^{\frac{3}{2}} + a_2$$
$$a_1, a_2 \in \mathbb{R} \tag{6.5}$$

The kinesthetic component in the contact interaction signature is described in equation 6.6 .

$$c_P = n_1 c_D^{\frac{3}{2}} + n_2$$
$$n_1, n_2 \in \mathbb{R} \tag{6.6}$$

The constants a_1, a_2 and n_1, n_2 are the cutaneous and kinesthetic interaction parameters, respectively. These parameters are different for each class of materials. They encode the signature of the dynamic behaviour of the material during a "press-and-release" exploration movement. The behaviour is related to the haptic properties of that material. The parameters can be used as descriptors of the class of the materials to discriminate objects made of different materials.

Given some data c_A, c_P, c_D resulting from a "press-and-release" exploration movement, the parameters a_1, a_2 and n_1, n_2 are estimated using the method MLE (Maximum Likelihood Estimation). The general goal of this method is to identify the parameters of the models presented in equations 6.5 and 6.6 which are most likely to have generated the set of data points c_A, c_P, c_D.

The next section presents the Bayesian model proposed in this chapter to discriminate different classes of materials.

6.6   Perception of the haptic stimulus map

This section proposes a Bayesian model to infer the perceived category of haptic stimulus (class of material) from the contact and kinesthetic interaction parameters extracted
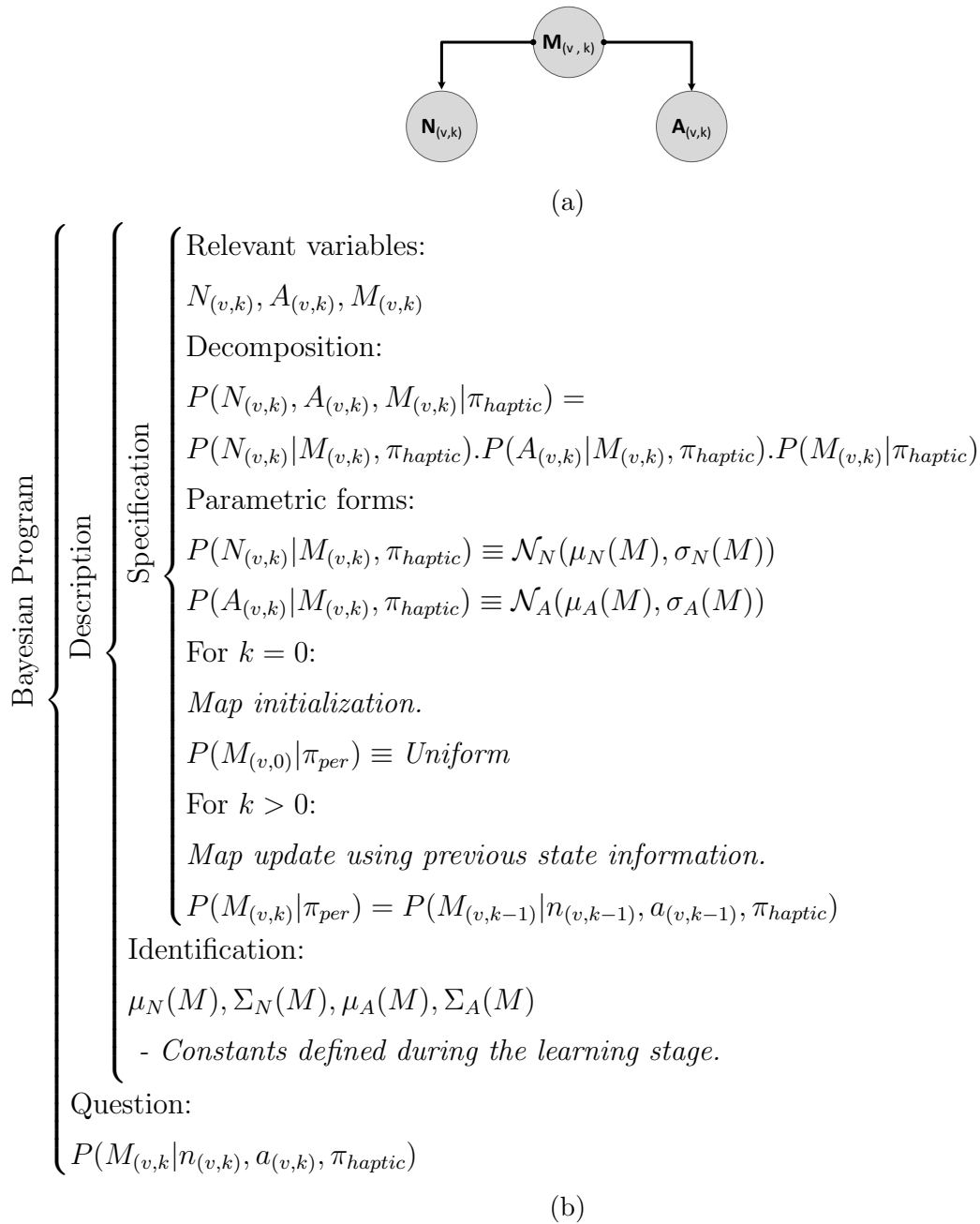
(a)

Relevant variables:

$N_{(v,k)}, A_{(v,k)}, M_{(v,k)}$

Decomposition:

$P(N_{(v,k)}, A_{(v,k)}, M_{(v,k)}|\pi_{haptic}) =$

$P(N_{(v,k)}|M_{(v,k)}, \pi_{haptic}).P(A_{(v,k)}|M_{(v,k)}, \pi_{haptic}).P(M_{(v,k)}|\pi_{haptic})$

Parametric forms:

$P(N_{(v,k)}|M_{(v,k)}, \pi_{haptic}) \equiv \mathcal{N}_N(\mu_N(M), \sigma_N(M))$

$P(A_{(v,k)}|M_{(v,k)}, \pi_{haptic}) \equiv \mathcal{N}_A(\mu_A(M), \sigma_A(M))$

For $k = 0$:

Map initialization.

$P(M_{(v,0)}|\pi_{per}) \equiv Uniform$

For $k > 0$:

Map update using previous state information.

$P(M_{(v,k)}|\pi_{per}) = P(M_{(v,k-1)}|n_{(v,k-1)}, a_{(v,k-1)}, \pi_{haptic})$

Identification:

$\mu_N(M), \Sigma_N(M), \mu_A(M), \Sigma_A(M)$

 - *Constants defined during the learning stage.*

Question:

$P(M_{(v,k}|n_{(v,k)}, a_{(v,k)}, \pi_{haptic})$

(b)

Figure 6.5: Bayesian model π_{haptic} *Perception of the haptic stimulus map.* a) Graphical representation. b) Bayesian program.

from the sensory data $\mathbf{h}_{(v,k)}$. The Bayesian model π_{haptic} is presented in Figure 6.5a and described in detail in the next sections.

6.6.1 Random variables of the model

The perceived category of the haptic stimulus is modelled by the discrete random variable $M_{(v,k)}$, as described in equation 6.7. N is the total number of different materials which can be discriminated by the system.

$$M_{(v,k)} - \text{"Material category of v"}$$
$$M_{(v,k)} \in \{Material_1, \dots, Material_N\} \tag{6.7}$$

In this Bayesian model, the information about the cutaneous contact interaction is integrated by the continuous random variable $A_{(v,k)}$, detailed in equation 6.8.

$$A_{(v,k)} - \text{"Cutaneous contact interaction parameters"}$$
$$A_{(v,k)} = (a_1, a_2)$$
$$A_{(v,k)} \in \mathbb{R}^2 \tag{6.8}$$

Conversely, the information encoded by the kinesthetic interaction parameters is described by the continuous random variable $N_{(v,k)}$, presented in equation 6.9.

$$N_{(v,k)} - \text{"Kinesthetic contact interaction parameters"}$$
$$N_{(v,k)} = (n_1, n_2)$$
$$N_{(v,k)} \in \mathbb{R}^2 \tag{6.9}$$

The description and methods used to determine the parameters a_1, a_2, n_1, n_2 from the haptic sensory data $\mathbf{h}_{(v,k)}$ are presented in section 6.5.2.

6.6.2 Inference of the haptic stimulus category

Figure 6.5a shows a graphical representation of the Bayesian model proposed in this chapter. It describes the statistical independence relationship between the random variables $M_{(v,k)}$, $A_{(v,k)}$ and $N_{(v,k)}$ of the model. Considering the relations presented in Figure 6.5a, the joint probability distribution function $P(M_{(v,k)}, N_{(v,k)}, A_{(v,k)}|\pi_{haptic})$ can be decom-

posed as presented in Figure 6.5b and equation 6.10.

$$P(M_{(v,k)}, N_{(v,k)}, A_{(v,k)}|\pi_{haptic}) =$$
$$= P(N_{(v,k)}|M_{(v,k)}, \pi_{haptic})P(A_{(v,k)}|M_{(v,k)}, \pi_{haptic})P(M_{(v,k)}|\pi_{haptic}) \quad (6.10)$$

The factors $P(N_{(v,k)}|M_{(v,k)}, \pi_{haptic})$ and $P(A_{(v,k)}|M_{(v,k)}, \pi_{haptic})$ express the likelihood of having specific measurements of kinestethic $n_{(v,k)}$ and cutaneous $a_{(v,k)}$ contact interaction parameters for a given type of material (haptic stimulus) $M_{(v,k)}$. $P(M_{(v,k)}|\pi_{haptic})$ is the *a-priori* probability of exploring a specific type of material.

The probability distribution function modelling the category of the haptic stimulus (type of material) is formulated from equation 6.10, as described in equation 6.11.

$$P(M_{(v,k)}|n_{(v,k)}, a_{(v,k)}, \pi_{haptic}) =$$
$$= \frac{P(n_{(v,k)}|M_{(v,k)}, \pi_{haptic})P(a_{(v,k)}|M_{(v,k)}, \pi_{haptic})P(M_{(v,k)}, \pi_{haptic})}{\sum\limits_{M_{(v,k)}} P(n_{(v,k)}|M_{(v,k)}, \pi_{haptic})P(a_{(v,k)}|M_{(v,k)}, \pi_{haptic})P(M_{(v,k)}, \pi_{haptic})} \quad (6.11)$$

The category of the haptic stimulus is inferred using the *Maximum a-Posteriori* (MAP) decision rule, as described in equation 6.12.

$$\hat{m}_{(v,k)} = \underset{m_{(v,k)}}{\arg\max} P(M_{(v,k)}|n_{(v,k)}, a_{(v,k)}, \pi_{haptic})$$
$$\hat{m}_{(v,k)} = \underset{m_{(v,k)}}{\arg\max} P(n_{(v,k)}|M_{(v,k)}, \pi_{haptic})P(a_{(v,k)}|M_{(v,k)}, \pi_{haptic})P(M_{(v,k)}|\pi_{haptic}) \quad (6.12)$$

Each of the factors involved in the inference of $\hat{m}_{(v,k)}$ is modelled by a probability distribution function presented in Figure 6.5b and detailed in section 6.6.3.

6.6.3 Determination of $P(N_{(v,k)}|M_{(v,k)}, \pi_{haptic})$ and $P(A_{(v,k)}|M_{(v,k)}, \pi_{haptic})$

The probability distribution functions $P(N_{(v,k)}|M_{(v,k)}, \pi_{haptic})$ and $P(A_{(v,k)}|M_{(v,k)}, \pi_{haptic})$ are normal probability distribution functions. Thus, both are modelled by bi-dimensional Gaussian functions as described by equations 6.13 and 6.14.

$$P(N_{(v,k)}|M_{(v,k)}, \pi_{haptic}) \equiv \mathcal{N}_N(\mu(M), \Sigma(M)) \quad (6.13)$$

$$P(A_{(v,k)}|M_{(v,k)}, \pi_{haptic}) \equiv \mathcal{N}_A(\mu(M), \Sigma(M)) \tag{6.14}$$

For each of the reference materials $M_{(v,k)}$ recognized by the system, the mean μ and covariance matrix Σ of the functions $\mathcal{N}_N$ and $\mathcal{N}_A$ are learned during a training period.

In this training period, a sample of each reference material recognized by the system is explored during several "press-and-release" movements. The (c_P, c_A, c_D) data acquired during each of the "press-and-release" cycles are used to determine the contact interaction parameters (a_1, a_2) and (n_1, n_2) for that material, using the Maximum Likelihood Estimation (MLE) method.

After a pre-defined number of press-and-release cycles, the average μ values of (a_1, a_2) and (n_1, n_2) are determined, as well as the respective covariance matrix Σ.

6.7 Post-processing of haptic stimulus map

As mentioned in the previous section, the haptic properties of the objects explored in the workspace are represented using a probabilistic (inference) grid. The formulation of this type of representation framework (analogous to an occupancy grid) considers that the representation of each grid cell v is independent from the remaining cells v of the grid (see details in section 2). This assumption frequently originates from unexplored grid cells having high uncertainty, even if those regions are surrounded by cells which were explored, having an informative haptic description assigned to them and thus a lower uncertainty.

This section proposes a method which is applied to the final haptic stimulus map provided by the Bayesian model π_{haptic} presented in section 6.6. The methods proposed in this chapter consider some constraints derived from the physical world. The physical world (explored object) has spatial structure; thus, it is expected to find local spatial continuity in the haptic perceptual characterization of contiguous grid cells.

The methods proposed in this section improve the perceptual representation of the haptic properties of the object by estimating the representation of unexplored grid cells based on the representation of neighbour cells which were explored.

The set of unexplored grid cells is defined by the variable ϑ_{unexpl}. The haptic description of an unexplored cell is estimated as the weighted mean of the haptic description of the eight grid cells surrounding that cell, as described in 6.15.

$$\forall_v \in \vartheta_{unexpl}, \quad P(M_{(v,k)}|N_{(v,k)}, A_{(v,k)}, \pi_{haptic}) = \frac{\sum_{j=1}^{8} \frac{1}{H(vj)} P(M_{(vj,k)}|N_{(vj,k)}, A_{(vj,k)}, \pi_{haptic})}{\sum_{j=1}^{8} \frac{1}{H(vj)}}$$

$$(6.15)$$

$H(vj)$ is the entropy of the grid cell vj (more details in chapter 2). The weights $\frac{1}{H(vj)}$ of the extrapolation method assign a higher contribution to the representation of grid cells with lower entropy $H(vj)$ (less uncertainty). vj represents each of the eight neighbour cells of v. The determination of the entropy of a random variable is detailed in section 2.

6.8 Experimental results

6.8.1 Experimental setup

The methods proposed in this work were tested using a human hand as exploration agent. The right hand of the participant was instrumented with a tactile sensing array *Tekscan Grip System* (Tekscan Inc, Boston, MA, U.S.) and a motion tracking system *Polhemus Liberty* (Polhemus Inc, Colchester, VT, U.S.). The instrumented hand is shown in Figure 6.6b.

The tactile sensing array is attached to the surface of the fingers using glue tape. It provides information about the spatial configuration of the regions of the hand contacting the object, the intensity, and the area of contact (cutaneous information). In this work, only one pad (array with $16 = 4 \times 4$ sensing elements) of the *Tekscan Grip System* is attached to the index fingertip (Figure 6.6b) (Figure 6.6a). The output of each sensing element of the array is an eight-bit integer. This work considers the raw outputs of the tactile sensing array without prior calibration. A method, called equilibration, proposed by the manufacturer of the system, is applied before each run of the data acquisition. The method is used to compensate for unexpected variations of the output between sensing elements. The data of each tactile sensing element is sampled at 50 Hz.

One sensor of the motion tracking device *Polhemus Liberty* was attached using glue tape to the same index fingertip of the tactile sensing array, as shown in Figure 6.6b. This motion tracking sensor provides information about the 6D pose (3D position, 3D orientation) of the fingertip and inherently of the tactile sensing array. This data provided the kinesthetic component of the interaction, related to the indentation depth of the fingertip in the natural shape of the object. The motion tracking sensor was sampled at approximately 30 Hz.

The multi-modal data samples were individually timestamped in millisecond *ms* reso-

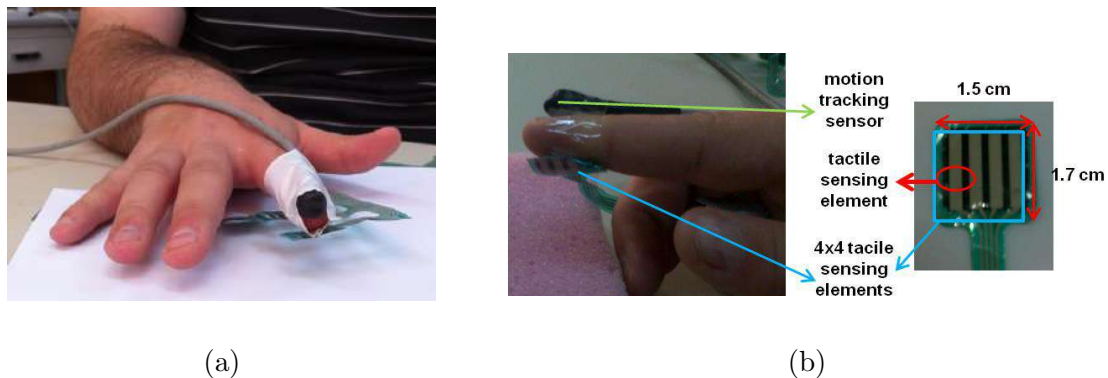(a)   (b)

Figure 6.6: Instrumented finger involved in the haptic exploration of objects. a) global overview. b) detailed view of the integration of the *Tekscan Grip* system and the motion tracking sensor *Polhemus Liberty*.

lution by the software applications developed for each of the data acquisition devices (see chapter 4). The clocks of the different computers involved in the architecture of the data acquisition were synchronized using Network Time Protocol (NTP) (see chapter 4).

6.8.2   Learning of the contact interaction parameters of the reference materials

Experimental protocol

During the learning stage of the contact interaction parameters (a_1, a_2), and (n_1, n_2), physical samples of three reference materials $Material_1$, $Material_2$, and $Material_3$ are selected and placed in the experimental area.

The samples selected for this work are presented in Figure 6.7. They were selected to represent common objects of daily life and to have distinct haptic properties. $Material_1$, $Material_2$, and $Material_3$ were evaluated empirically by a human operator (exploration using a non-instrumented human hand) and have increasing levels of perceived hardness, respectively.

Each of the reference materials $Material_1$, $Material_2$, and $Material_3$ was submitted to ten press-and-release exploration cycles using the index fingertip of the instrumented hand, as presented in Figure 6.6b. All the press-and-release exploration cycles were performed in the same region of the surface of the object. Thus, the subject applies a unidirectional movement perpendicular to the natural shape of the physical samples of the reference materials (Figure 6.7d).
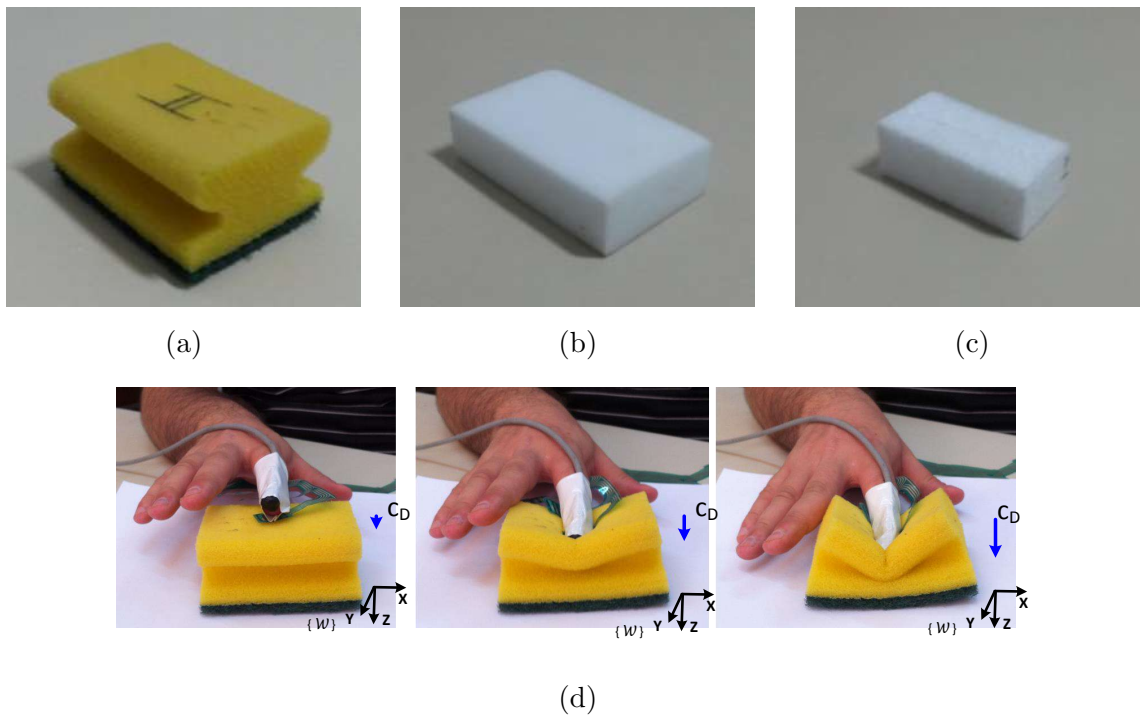
(a)   (b)   (c)

(d)

Figure 6.7: Reference materials a) $Material_1$. b) $Material_2$. c)$Material_3$. d) Demonstration of the press-and-release exploration pattern.

Estimation of $P(N_{(v,k)}|M_{(v,k)}, \pi_{haptic})$ **and** $P(A_{(v,k)}|M_{(v,k)}, \pi_{haptic})$

The contact sensing features c_P, c_A, and c_D extracted from the haptic sensory data $\mathbf{h}_{(v,k)}$ during all ten press-and-release exploration movements are presented in Figure 6.8, 6.9, and 6.10, for each of the reference materials $Material_1$, $Material_2$, and $Material_3$, respectively.

For all the reference materials, during each of the ten press-and-release movements, as the press segment of the movement progresses, the contact intensity c_P, contact area c_A, and contact indentation level c_D increase, as long as the press movements progress. During the release segment, they decrease. This work only uses segments from the press exploration movements. The contact sensing features c_P, c_A, c_D from the ten press segments of the press-and-release cycles for $Material_1$, $Material_2$, and $Material_3$ are represented in Figure 6.11.

However, although the global behaviour is analogous, each of the reference materials has its own characteristic profile. That unique profile is specified by the contact interaction cutaneous (a_1, a_2) and kinesthetic (n_1, n_2) parameters.

For each of the press segments of the press-and-release exploration movement, the parameters (a_1, a_2) and (n_1, n_2) were estimated using the *MATLAB Curve Fitting Toolbox* (The MathWorks Inc, MA, U.S.). The results are shown in Table 6.3, Table 6.4, and Table 6.5, for $Material_1$, $Material_2$, and $Material_3$, respectively. The curve fitting errors, sum
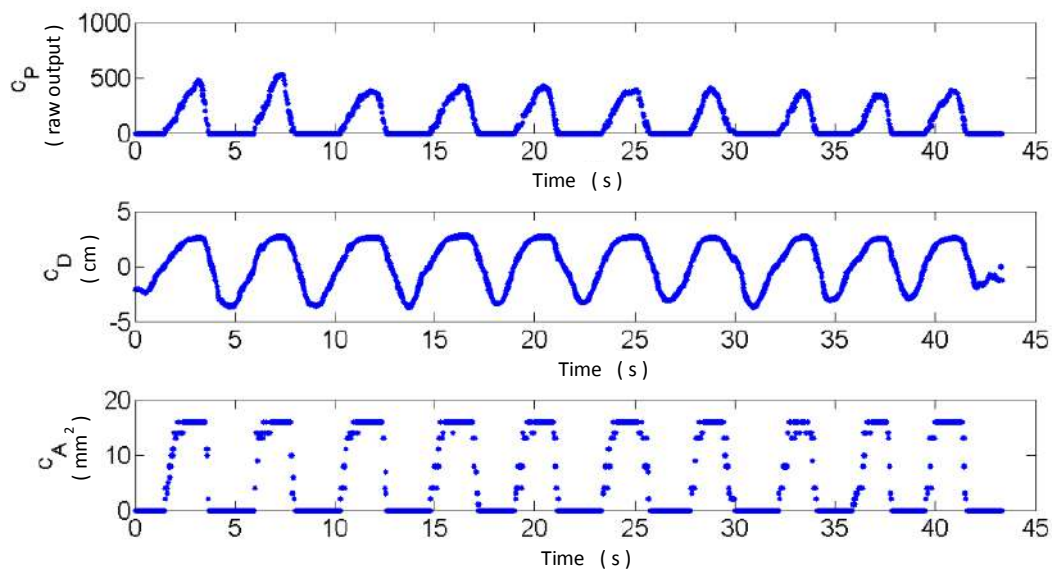
Figure 6.8: Typical temporal profile of the variables c_P, c_A, and c_D during ten press-and-release exploration movements of $Material_1$.
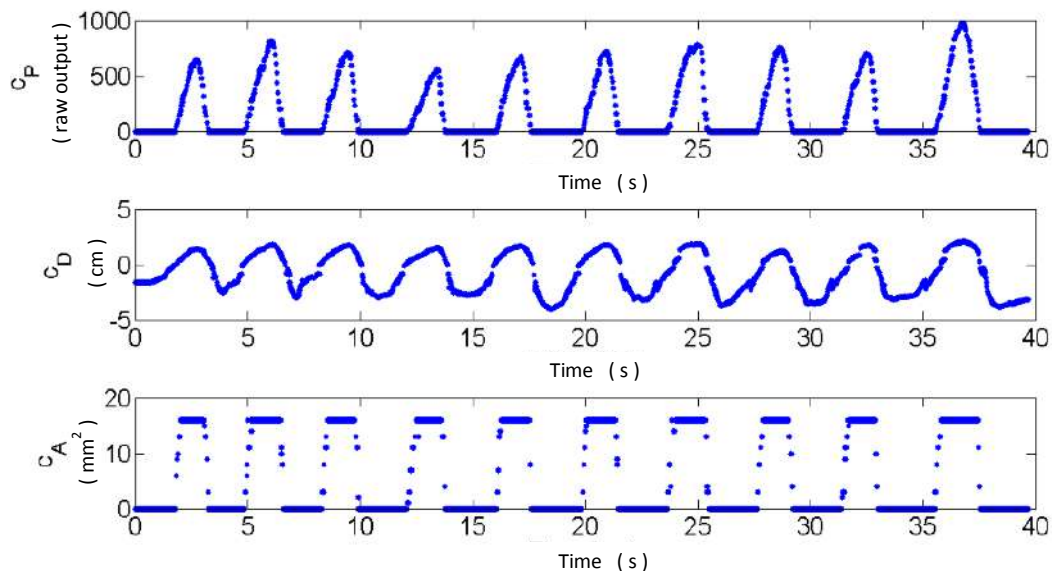

Figure 6.9: Typical temporal profile of the variables c_P, c_A, and c_D during ten press-and-release exploration movements of $Material_2$.
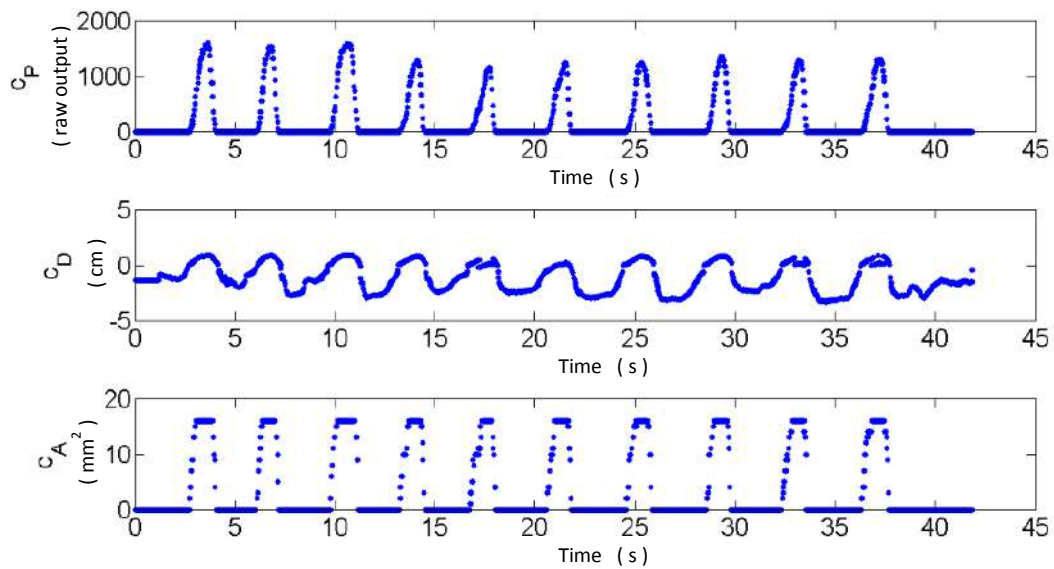
Figure 6.10: Typical temporal profile of the variables c_P, c_A, and c_D during ten press-and-release exploration movements of $Material_3$.
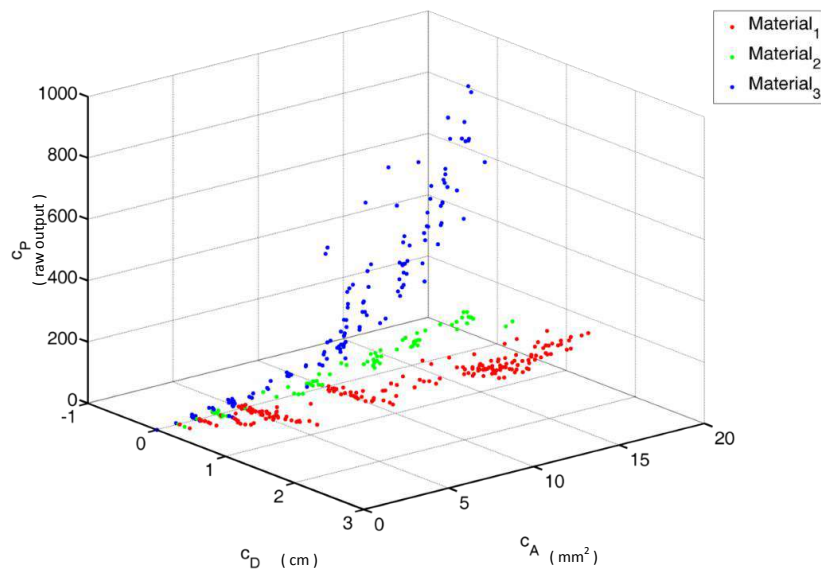

Figure 6.11: Typical contact interaction profile (c_P, c_A, c_D) of $Material_1$, $Material_2$, $Material_3$.

Table 6.3: Contact interaction parameters $N_{(v,k)}$ (kinesthetic) and $A_{(v,k)}$ (cutaneous) for $Material_1$

Exploration	$N_{(v,k)}$			$A_{(v,k)}$		
Run	n_1	n_2	Φ_N	a_1	a_2	Φ_A
1	83.1	15.6	7706.7	2.9	10.1	12997.9
2	66.7	18.7	9977.2	3.4	2.8	19108.7
3	70.1	19.8	4518.4	3.2	2.3	8505.6
4	74.2	11.8	6777.1	3.3	14.5	5485.2
5	66.4	10.5	4493.4	3.0	20.9	5285.1
6	67.4	10.8	4868.4	3.1	14.1	3389.3
7	66.7	18.8	6408.7	3.6	15.1	15691.7
8	102.4	19.1	3109.7	2.6	18.9	1773.5
9	82.8	-2.8	2793.3	2.8	17.4	3036.6
10	72.6	16.9	5570.4	2.3	18.5	3750.4

Table 6.4: Contact interaction parameters $N_{(v,k)}$ (kinesthetic) and $A_{(v,k)}$ (cutaneous) for $Material_2$

Exploration	$N_{(v,k)}$			$A_{(v,k)}$		
Run	n_1	n_2	Φ_N	a_1	a_2	Φ_A
1	493.6	30.2	1715.9	3.0	-0.7	415.4
2	467.9	-3.4	2147.5	2.8	12.1	5172.4
3	380.4	-7.7	1989.5	2.9	5.5	1182.3
4	436.0	-16.9	3571.0	2.9	0.1	1290.9
5	679.7	7.9	625.6	2.4	7.3	572.4
6	604.2	-1.3	450.5	2.8	0.0	1372.9
7	525.9	4.0	4496.3	2.1	14.4	446.1
8	177.2	38.9	9807.9	3.8	-9.7	2282.8
9	385.8	4.6	1723.4	3.1	6.4	389.9
10	175.5	40.0	8935.9	3.0	-0.2	818.8

Table 6.5: Contact interaction parameters $N_{(v,k)}$ (kinesthetic) and $A_{(v,k)}$ (cutaneous) for $Material_3$

Exploration	$N_{(v,k)}$			$A_{(v,k)}$		
Trial	n_1	n_2	Φ_N	a_1	a_2	Φ_A
1	2030.4	-31.2	5091.9	10.6	-64.7	70064.9
2	952.6	-112.6	69435.6	10.1	-48.1	35691.9
3	1858.4	-30.2	31394.8	12.9	-117.7	165029.3
4	2144.5	-48.8	26389.5	11.2	-91.4	132650.9
5	183.6	213.1	671769.1	10.5	-44.2	101726.5
6	2154.0	-17.1	13875.6	9.8	-37.2	36101.0
7	2128.4	-8.0	19706.1	12.2	-91.1	239131.8
8	2204.5	-14.4	8201.4	10.6	-69.5	104792.6
9	1818.9	-45.8	19224.5	10.9	-73.1	103725.3
10	1357.5	68.1	410851.5	10.3	-59.8	164797.7

Table 6.6: LearMean (μ) and co-variation matrix (Σ) parameters learned from the data in Table 6.3, Table 6.4, and Table 6.5

Parameters	$Material_1$		$Material_2$		$Material_3$	
μ_N	$(75.2$	$13.9)$	$(432.6$	$9.6)$	$(1638.3$	$-2.7)$
Σ_N	$\begin{pmatrix} 117.4 & -3.5 \\ -3.5 & 42.5 \end{pmatrix}$		$\begin{pmatrix} 24042.6 & -1626.1 \\ -1626.1 & 356.2 \end{pmatrix}$		$\begin{pmatrix} 396276.5 & -32354.7 \\ -32354.7 & 6959.4 \end{pmatrix}$	
μ_A	$(3.0$	$12.5)$	$(2.9$	$3.5)$	$(10.9$	$-69.7)$
Σ_A	$\begin{pmatrix} 0.1 & -1.1 \\ -1.1 & 38.1 \end{pmatrix}$		$\begin{pmatrix} 0.2 & -2.4 \\ -2.4 & 44.9 \end{pmatrix}$		$\begin{pmatrix} 0.8 & -20.2 \\ -20.2 & 554.2 \end{pmatrix}$	

of squared 2-norm of the residuals, are represented by the variables Φ_N and Φ_A and reported in Table 6.3, Table 6.4, and Table 6.5. The determination of Φ_N and Φ_A is described in equations 6.16 and 6.17. S represents the number of sensory samples used in each trial as input to the curve fitting method.

$$\Phi_N = \sum_{i=1}^{S}(c_{P,i} - (\hat{n}_1 c_{D,i}^{\frac{3}{2}} + \hat{n}_2))^2 \tag{6.16}$$

$$\Phi_A = \sum_{i=1}^{S}(c_{P,i} - (\hat{a}_1 c_{A,i}^{\frac{3}{2}} + \hat{a}_2))^2 \tag{6.17}$$

The results in Tables 6.3, 6.4, and 6.5 are used to determine the parameters average μ_A, μ_N and co-variance matrices Σ_A, Σ_N for each of the reference materials, as presented in Table 6.6. These parameters, which are learned from the training data, are used to specify the probability distribution functions $P(N_{(v,k)}|M_{(v,k)}, \pi_{haptic})$ and $P(A_{(v,k)}|M_{(v,k)}, \pi_{haptic})$, represented in Figure 6.12, Figure 6.13, and Figure 6.14.

The probability distribution functions are used in section 6.8.3 to infer the haptic properties of objects unknown to the system.

Evaluating the learned parameters of $P(N_{(v,k)}|M_{(v,k)}, \pi_{haptic})$ and $P(A_{(v,k)}|M_{(v,k)}, \pi_{haptic})$

The evaluation of the probability distribution functions $P(N_{(v,k)}|M_{(v,k)}, \pi_{haptic})$ and $P(A_{(v,k)}|M_{(v,k)}, \pi_{haptic})$ learned from the experimental data is performed following the cross-validation scheme leave-one-out. For each reference material, $P(N_{(v,k)}|M_{(v,k)}, \pi_{haptic})$ and $P(A_{(v,k)}|M_{(v,k)}, \pi_{haptic})$ are learned from nine of the ten press segments of the press-and-release exploration movements and tested for the remaining. The categorization of the sample (n_1, n_2), (a_1, a_2) is made according to equation 6.18.
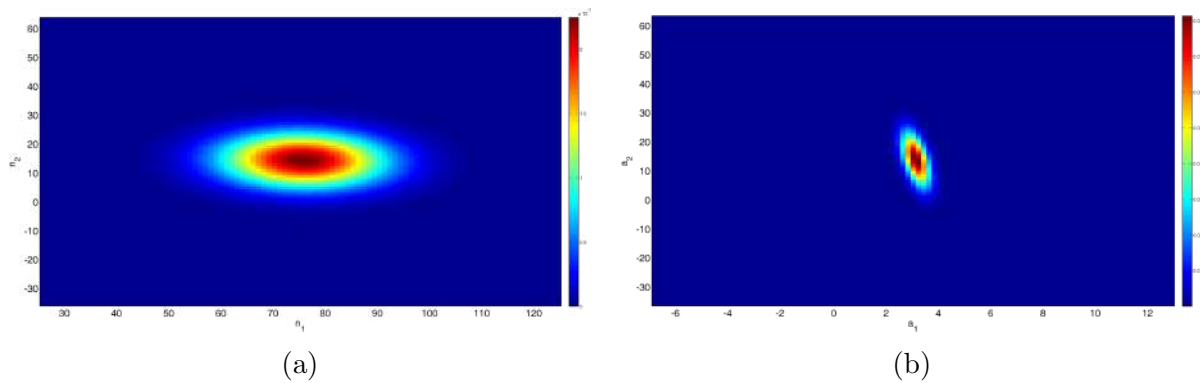
Figure 6.12: Graphical representation of the probability distribution functions learned from $Material_1$ data. a) $P(N_{(v,k)}|M_{(v,k)}, \pi_{haptic})$. b) $P(A_{(v,k)}|M_{(v,k)}, \pi_{haptic})$.
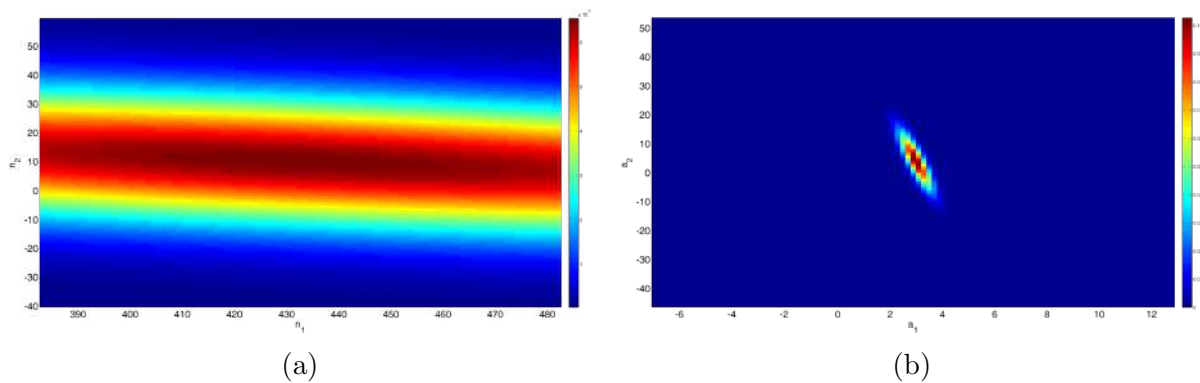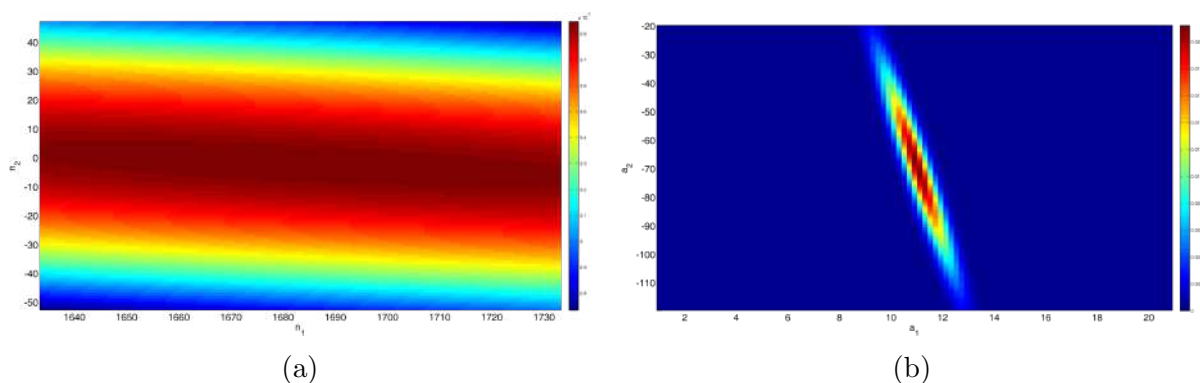

Figure 6.13: Graphical representation of the probability distribution functions learned from $Material_2$ data. a) $P(N_{(v,k)}|M_{(v,k)}, \pi_{haptic})$. b) $P(A_{(v,k)}|M_{(v,k)}, \pi_{haptic})$.

Figure 6.14: Graphical representation of the probability distribution functions learned from $Material_3$ data. a) $P(N_{(v,k)}|M_{(v,k)}, \pi_{haptic})$. b) $P(A_{(v,k)}|M_{(v,k)}, \pi_{haptic})$.

Table 6.7: Confusion table for the categorization of $Material_i$ (ground truth) as $M.i$ (perceived category) by the Bayesian model π_{haptic}, using a leave-one-out cross-validation scheme

	$M.1$	$M.2$	$M.3$
$Material_1$	0.82	0.18	0.00
$Material_2$	0.00	1.00	0.00
$Material_3$	0.00	0.00	1.00

(a)   (b)   (c)
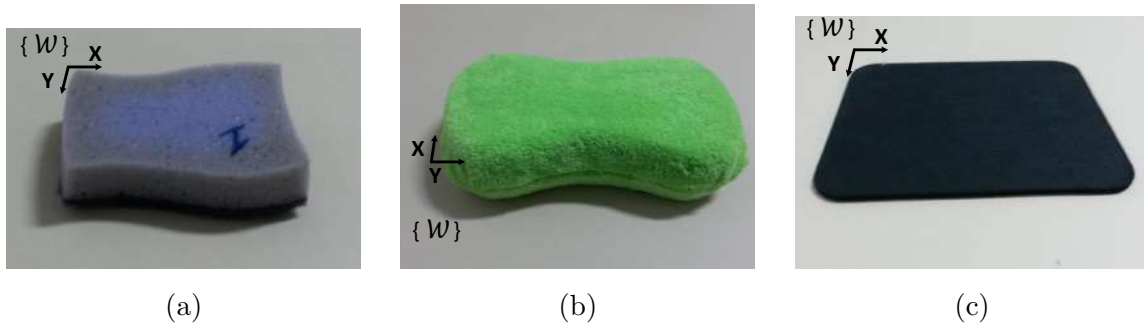
Figure 6.15: Unknown objects a) $Object_1$ b) $Object_2$ c)$Object_3$.

$$\hat{m}_{(v,k)} = \arg\max_{m_{(v,k)}} P(n_{(v,k)}|M_{(v,k)}, \pi_{haptic}) P(a_{(v,k)}|M_{(v,k)}, \pi_{haptic}) P(M_{(v,k)}|\pi_{haptic}) \quad (6.18)$$

Table 6.7 presents the confusion table resulting for the cross-validation of the Bayesian model π_{haptic} following a leave-one-out scheme.

The results presented in Table 6.7 show that the proposed Bayesian model π_{haptic} has a high capability to discriminate the proposed reference materials. The model shows only a minimal confusion in the discrimination of $Material_1$ and $Material_2$.

6.8.3 Haptic exploration of unknown objects

Experimental protocol

After the learning stage of the Bayesian model π_{haptic} for the reference materials $Material_1$, $Material_2$, and $Material_3$, the model π_{haptic} can be used to infer the similarity of haptic properties of new objects unknown to the system with the reference materials previously learned by the system. This work proposes the haptic exploration of three new objects, $Object_1$, $Object_2$, and $Object_3$, presented in Figures A, B, and C, respectively.

The workspace region is partitioned on a bi-dimensional inference grid. Each cell is a square of $1cm$ side. Each of the new objects is placed in this workspace region and explored in five pre-defined regions of the surface, using a total of ten press-and-release exploration movements (two press-and-release movements per region). The list of five

Table 6.8: Pre-defined coordinates of the cells on the grid where the press-and-release exploration movements are performed

	$Object_1$	$Object_2$	$Object_3$
$Region_1$	(3,3)	(5,5)	(3,3)
$Region_2$	(4,6)	(12,7)	(4,6)
$Region_3$	(3,8)	(5,8)	(3,8)
$Region_4$	(5,3)	(20,5)	(5,3)
$Region_5$	(5,8)	(20,8)	(5,8)
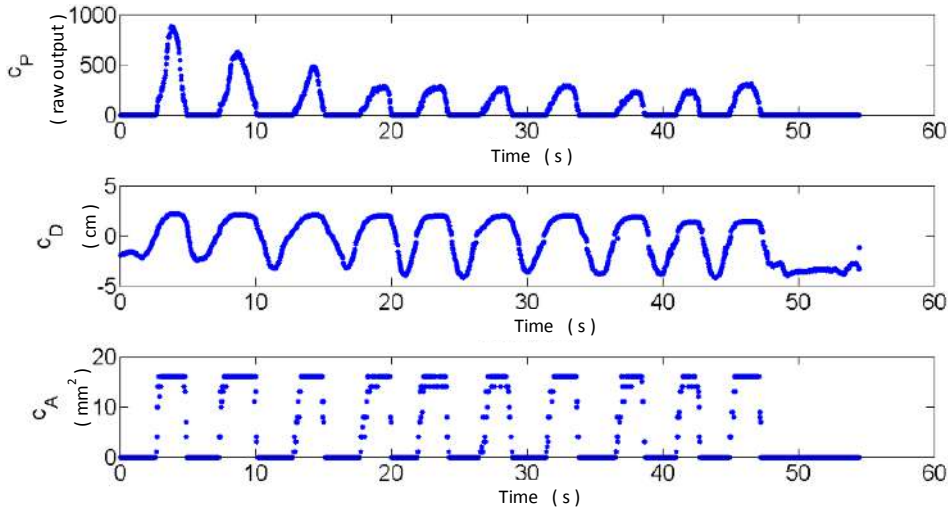
Figure 6.16: Typical temporal profile of the variables c_P, c_A and c_D during press-and-release exploration movements of $Object_1$.

pre-defined regions is proposed in Table 6.8.

The hand of the subject performing the haptic exploration of the new objects is instrumented with the same tactile sensing array *Tekscan Grip System* and motion tracking sensor *Polhemus Liberty*, as presented in Figure 6.6b.

Representation and update of the haptic stimulus map of unknown objects

The profile of the contact sensing features c_P, c_A, c_D (gathering the data from the ten exploration movements) of each of the new objects is presented in Figures 6.19, 6.20, and 6.21.

The temporal evolution of the haptic representation of each of the unknown objects $Object_1$, $Object_2$, and $Object_3$ is illustrated in Figures 6.23, 6.24, and 6.25 and detailed in Tables 6.9, 6.9, and 6.9. Initially, $(k = 0)$, and all the cells v of the workspace are described by a uniform probability distribution function $P(M_{(v,k)}|A_{(v,k)}, N_{(v,k)}, \pi_{haptic}) \equiv Uniform$. As long as the exploration of the unknown objects progresses $(k = 1, \ldots, k = 10)$ in the pre-defined regions listed in Table 6.8, the representation of those regions improves
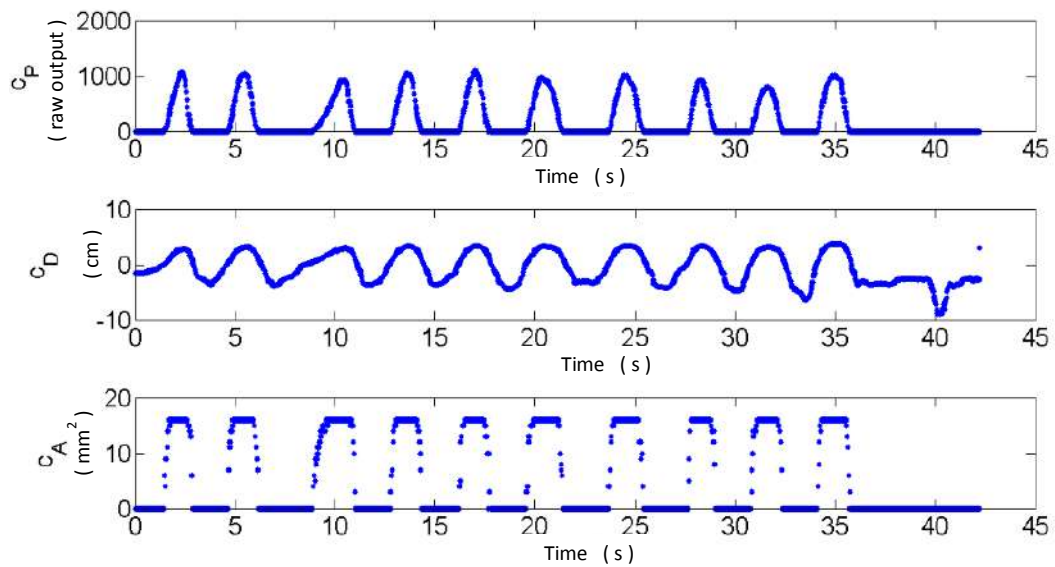
Figure 6.17: Typical temporal profile of the variables c_P, c_A and c_D during press-and-release exploration movements of $Object_2$.
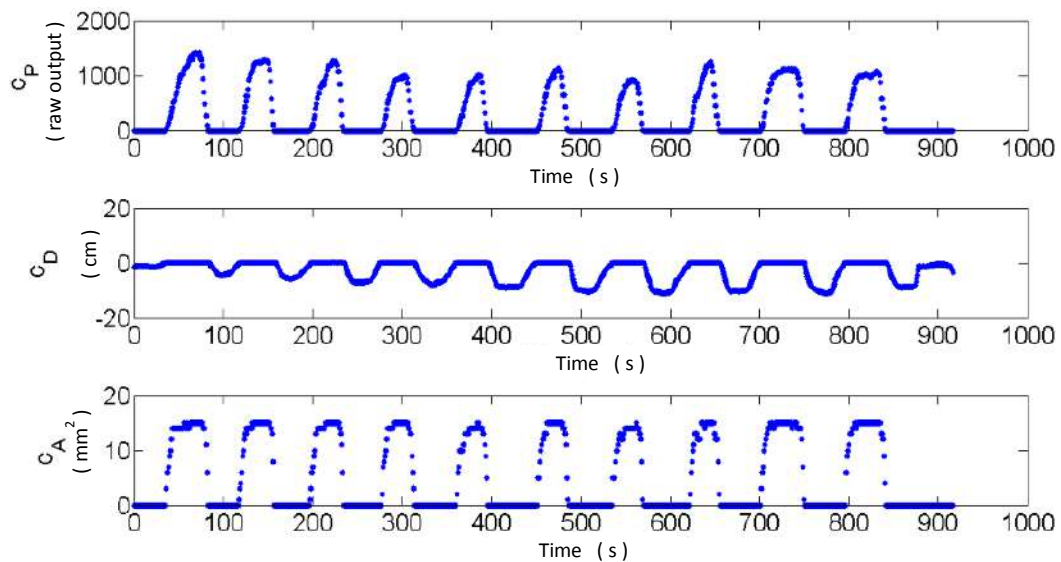

Figure 6.18: Typical temporal profile of the variables c_P, c_A and c_D during press-and-release exploration movements of $Object_3$.
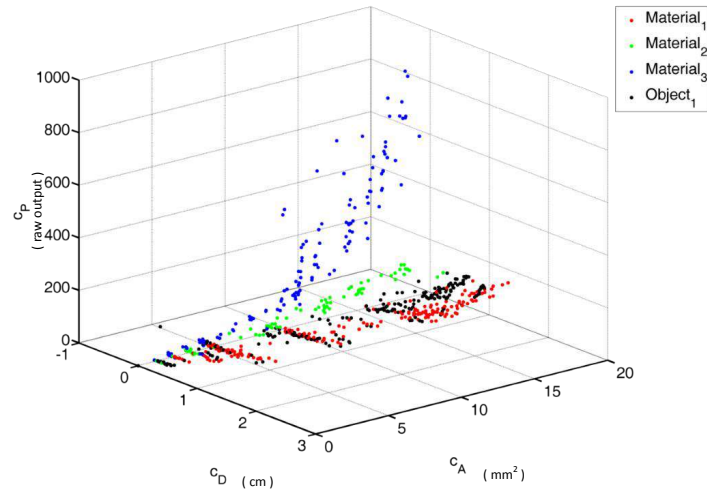
Figure 6.19: Typical contact interaction profile (c_P, c_A, c_D) of $Object_1$, compared with $Material_1$, $Material_2$, $Material_3$.
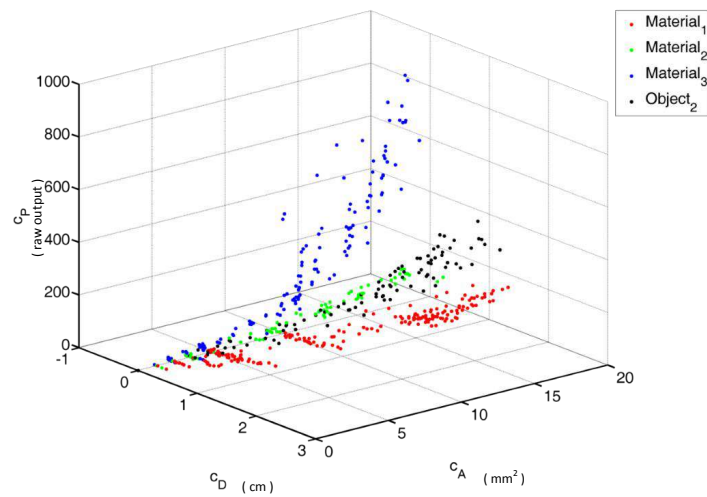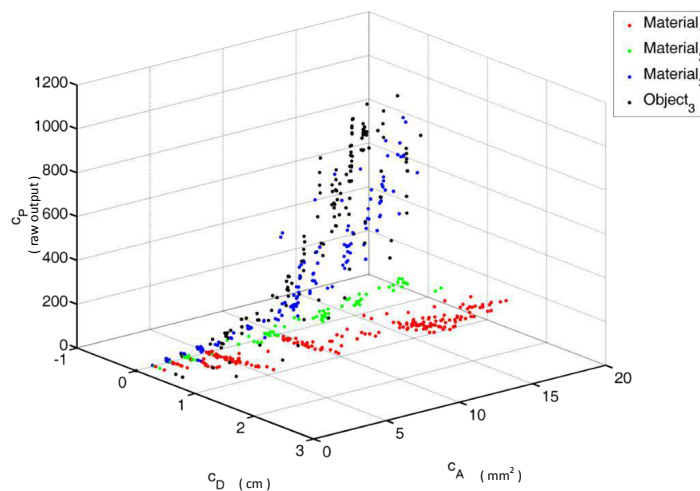

Figure 6.20: Typical contact interaction profile (c_P, c_A, c_D) of $Object_2$, compared with $Material_1$, $Material_2$, $Material_3$.

Figure 6.21: Typical contact interaction profile (c_P, c_A, c_D) of $Object_3$, compared with $Material_1$, $Material_2$, $Material_3$.

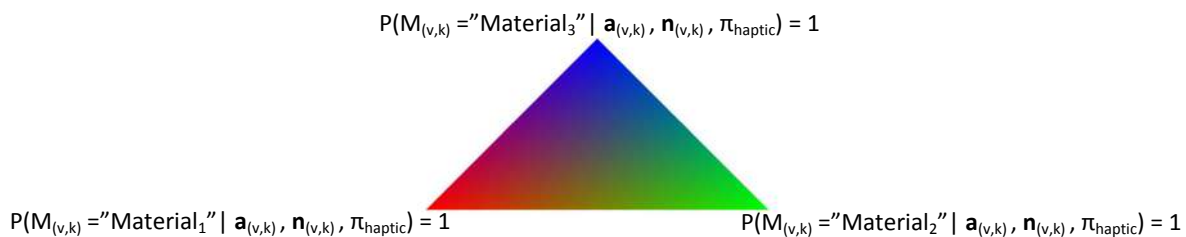Figure 6.22: Colormap used to represent $P(M_{(v,k)}|N_{(v,k)}, A_{(v,k)}, \pi_{haptic})$.

remarkably.

The regions of $Object_1$ are described as being similar (higher probability) to $Material_1$. Some of these regions improve their representation by integrating additional haptic data acquired in the exploration cycles. Two of the regions of $Object_1$ show a contact interaction behaviour recognized as $Material_2$.

Alternatively, all the explored regions of $Object_2$ and $Object_3$ are described as being made of materials with a contact interaction behaviour similar to $Material_2$ and $Material_3$, respectively. Since the initial exploration cycles, that tendency is evident.

Extrapolation of the representation of unexplored grid ells

The final representation of the workspace of $Object_1$, $Object_2$, and $Object_3$ are processed in an effort to improve the representation of the unexplored cells. The method presented in section 6.7 intends to reduce the uncertainty of the representation of the workspace by reducing the entropy of the representation. The results are shown in Figure 6.26.

By comparing Figures 6.23c, 6.24c, 6.25c, and 6.26, the extension of uncertain regions is reduced. The extension of regions characterized as being similar to $Material_1$,
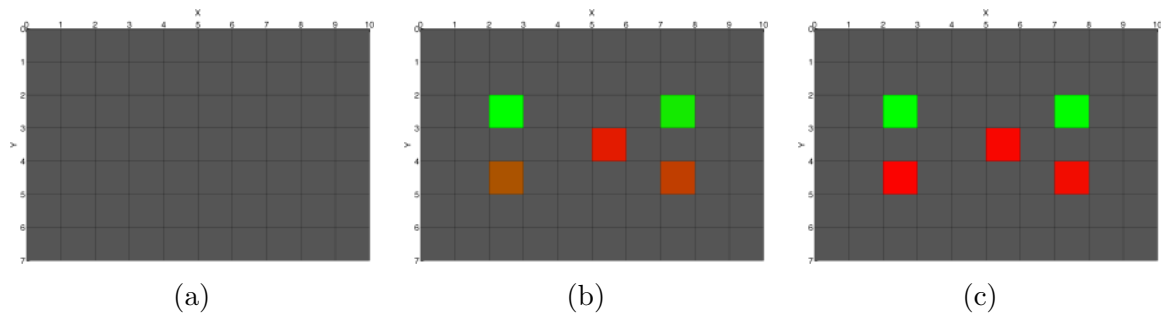
Figure 6.23: Probabilist representation of the result of the haptic exploration of $Object_1$. a) Initial representation ($k = 0$). b) Representation after five press-and-release movements ($k = 5$). c) Representation after five press-and-release movements ($k = 10$). Colormap described in Figure 6.22.

Figure 6.24: Probabilist representation of the result of the haptic exploration of $Object_1$. a) Initial representation ($k = 0$). b) Representation after five press-and-release movements ($k = 5$). c) Representation after five press-and-release movements ($k = 10$). Colormap described in Figure 6.22.
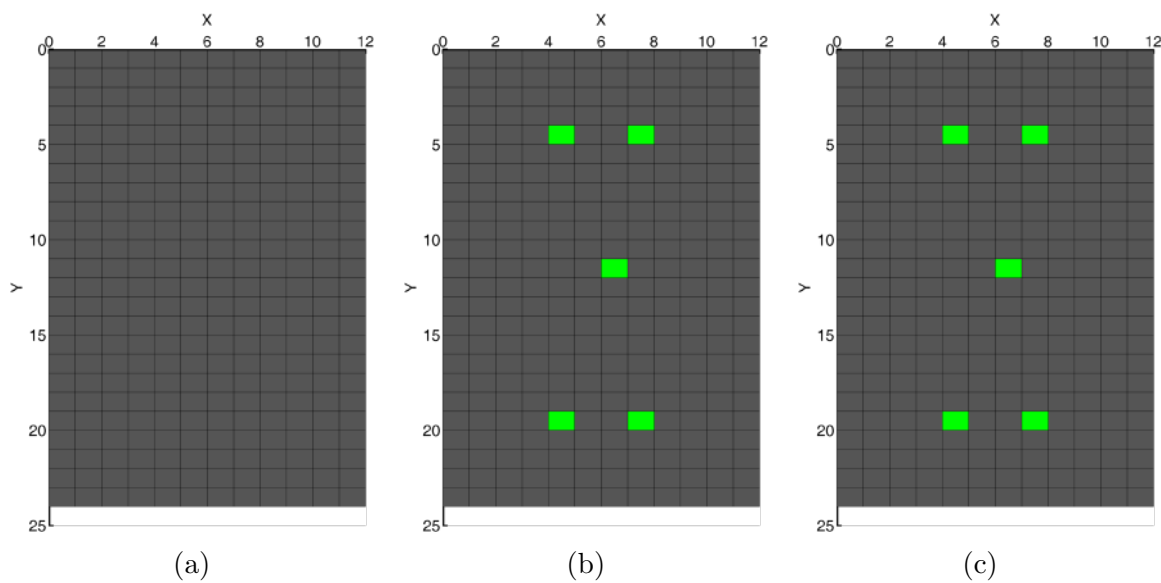

Figure 6.25: Probabilist representation of the result of the haptic exploration of $Object_1$. a) Initial representation ($k = 0$). b) Representation after five press-and-release movements ($k = 5$). c) Representation after five press-and-release movements ($k = 10$). Colormap described in Figure 6.22.
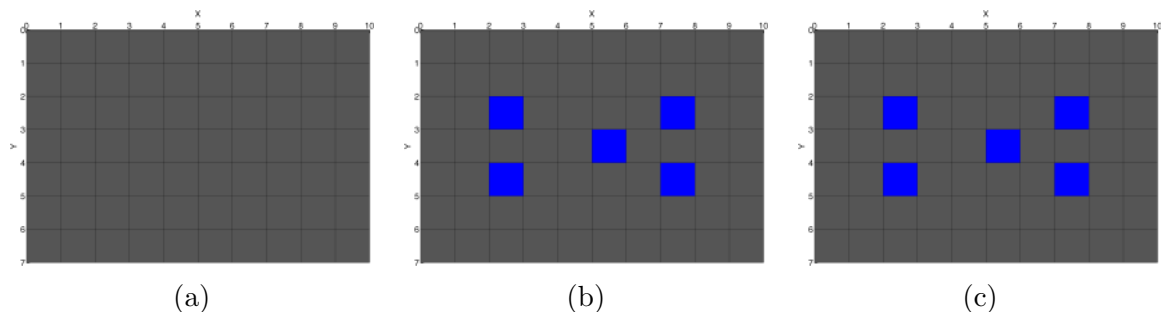
Table 6.9: Evolution of the probability distribution function $P(M_{(v,k)}|n_{(v,k)}, a_{(v,k)}, \pi_{haptic})$ during the exploration of $Object_1$

	Initial condition $(k = 0)$			1st exploration cycle $(k = 1, \ldots, 5)$			2nd exploration cycle $(k = 6, \ldots, 10)$		
	$Mat._1$	$Mat._2$	$Mat._3$	$Mat._1$	$Mat._2$	$Mat._3$	$Mat._1$	$Mat._2$	$Mat._3$
$Region_1$	0.33	0.33	0.33	0.01	0.99	0.00	0.00	1.00	0.00
$Region_2$	0.33	0.33	0.33	0.89	0.11	0.00	0.97	0.03	0.00
$Region_3$	0.33	0.33	0.33	0.08	0.92	0.00	0.01	0.99	0.00
$Region_4$	0.33	0.33	0.33	0.67	0.33	0.00	0.98	0.02	0.00
$Region_5$	0.33	0.33	0.33	0.75	0.25	0.00	0.95	0.05	0.00

Note: For simplicity and compactness of the notation, $Mat._1$, $Mat._2$, and $Mat._3$ were used to designate $Material_1$, $Material_2$, and $Material_3$, respectively.

Table 6.10: Evolution of the probability distribution function $P(M_{(v,k)}|n_{(v,k)}, a_{(v,k)}, \pi_{haptic})$ during the exploration of $Object_2$

	Initial condition $(k = 0)$			1st exploration cycle $(k = 1, \ldots, 5)$			2nd exploration cycle $(k = 6, \ldots, 10)$		
	$Mat._1$	$Mat._2$	$Mat._3$	$Mat._1$	$Mat._2$	$Mat._3$	$Mat._1$	$Mat._2$	$Mat._3$
$Region_1$	0.33	0.33	0.33	0.00	1.00	0.00	0.00	1.00	0.00
$Region_2$	0.33	0.33	0.33	0.00	1.00	0.00	0.00	1.00	0.00
$Region_3$	0.33	0.33	0.33	0.00	1.00	0.00	0.00	1.00	0.00
$Region_4$	0.33	0.33	0.33	0.00	1.00	0.00	0.00	1.00	0.00
$Region_5$	0.33	0.33	0.33	0.01	0.99	0.00	0.00	1.00	0.00

Note: For simplicity and compactness of the notation, $Mat._1$, $Mat._2$, and $Mat._3$ were used to designate $Material_1$, $Material_2$, and $Material_3$, respectively.

Table 6.11: Evolution of the probability distribution function $P(M_{(v,k)}|n_{(v,k)}, a_{(v,k)}, \pi_{haptic})$ during the exploration of $Object_3$

	Initial condition $(k = 0)$			1st exploration cycle $(k = 1, \ldots, 5)$			2nd exploration cycle $(k = 6, \ldots, 10)$		
	$Mat._1$	$Mat._2$	$Mat._3$	$Mat._1$	$Mat._2$	$Mat._3$	$Mat._1$	$Mat._2$	$Mat._3$
$Region_1$	0.33	0.33	0.33	0.00	0.00	1.00	0.00	0.00	1.00
$Region_2$	0.33	0.33	0.33	0.00	0.00	1.00	0.00	0.00	1.00
$Region_3$	0.33	0.33	0.33	0.00	0.00	1.00	0.00	0.00	1.00
$Region_4$	0.33	0.33	0.33	0.00	0.00	1.00	0.00	0.00	1.00
$Region_5$	0.33	0.33	0.33	0.00	0.00	1.00	0.00	0.00	1.00

Note: For simplicity and compactness of the notation, $Mat._1$, $Mat._2$, and $Mat._3$ were used to designate $Material_1$, $Material_2$, and $Material_3$, respectively.
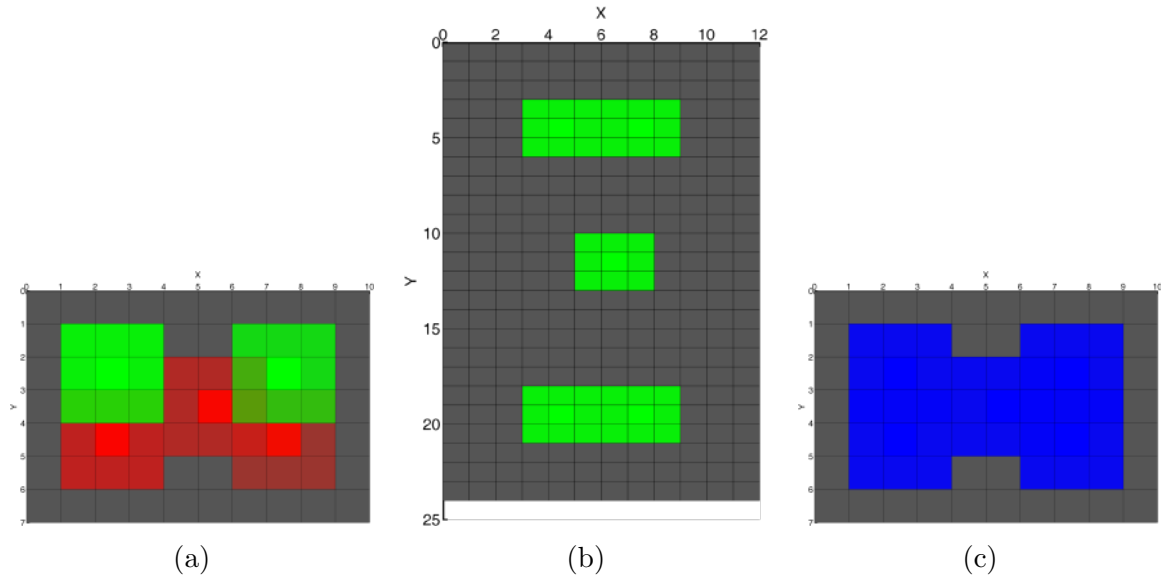
Figure 6.26: Probabilist representation of the result of the haptic exploration and post-processing of a) $Object_1$. b) $Object_2$. c) $Object_3$. Colormap described in Figure 6.22.

$Material_2$, or $Material_3$ increases. This methodology can be used, not only to improve the representation of the workspace, but also to speed up the exploration of the workspace toward an optimal representation.

6.9   Conclusions

The work presented in this chapter contributed to the development of autonomous dexterous robotic hand platforms by proposing a probabilistic inference grid to represent and discriminate the perceived hardness-softness characteristics extracted during the exploration of soft objects. The proposed approach follows some principles inspired by human strategies to perceive and estimate the haptic characteristics of objects in uncertain environments. The perceived hardness-softness characteristics of unknown objects are described by a probabilistic combination of previously known characteristics of a set of reference materials (haptic memory of the system).

This approach is designed to progressively receive haptic inputs (cutaneous and kinesthetic data). As long as the object exploration progresses, the total entropy of the representation is reduced, showing that the representation becomes less uncertain. The processing stages related to the integration of local context information have also contributed to the improvement of the representation.

Bibliography

[Bohg, 2011] Bohg, J. (2011). *Multi-Modal Scene Understanding for Robotic Grasping*. PhD thesis, KTH, Computer Vision and Active Perception, CVAP, Centre for Autonomous Systems, CAS.

[Chitta et al., 2011] Chitta, S., Sturm, J., Piccoli, M., and Burgard, W. (2011). Tactile sensing for mobile manipulation. *Robotics, IEEE Transactions on*, 27(3):558 –568.

[Dufour et al., 2011] Dufour, A., Thibeaux, R., Labruyere, E., Guillen, N., and Olivo-Marin, J.-C. (2011). 3-d active meshes: Fast discrete deformable models for cell tracking in 3-d time-lapse microscopy. *Image Processing, IEEE Transactions on*, 20(7):1925 – 1937.

[Faria et al., 2012] Faria, D. R., Martins, R., Lobo, J., and Dias, J. (2012). Extracting data from human manipulation of objects towards improving autonomous robotic grasping. *Robotics and Autonomous Systems*, 60(3):396 – 410.

[Feix et al., 2014] Feix, T., Bullock, I., and Dollar, A. (2014). Analysis of human grasping behavior: Object characteristics and grasp type. *Haptics, IEEE Transactions on*, 7(3):311–323.

[Fishel and Loeb, 2012] Fishel, J. A. and Loeb, G. E. (2012). Bayesian exploration for intelligent identification of textures. *Frontiers Neurorobotics*, 6.

[Frank et al., 2010] Frank, B., Schmedding, R., Stachniss, C., Teschner, M., and Burgard, W. (2010). Learning the elasticity parameters of deformable objects with a manipulation robot. In *Intelligent Robots and Systems (IROS), 2010 IEEE/RSJ International Conference on*, pages 1877 –1883.

[Garre et al., 2011] Garre, C., Hernández, F., Gracia, A., and Otaduy, M. A. (2011). Interactive simulation of a deformable hand for haptic rendering. In *Proc. of World Haptics Conference*. IEEE.

[Hongbin Liu, 2011] Hongbin Liu, Xiaojing Song, T. N. K. A. L. S. (2011). Friction estimation based object surface classification for intelligent manipulation. In *Proceddings

of *IEEE International Conference on Robotics and Automation 2011 (ICRA 2011) - Workshop on Autonomous Grasping.*

[Hui and Kuchenbecker, 2014] Hui, J. C. T. and Kuchenbecker, K. J. (2014). *Evaluating the BioTac's Ability to Detect and Characterize Lumps in Simulated Tissue*, pages 295–302. Springer Berlin Heidelberg, Berlin, Heidelberg.

[Lederman and Klatzky, 1987] Lederman, S. J. and Klatzky, R. L. (1987). Hand movements: A window into haptic object recognition. *Cognitive Psychology*, 19(3):342 – 368.

[Liu et al., 2010] Liu, H., Noonan, D., Challacombe, B., Dasgupta, P., Seneviratne, L., and Althoefer, K. (2010). Rolling mechanical imaging for tissue abnormality localization during minimally invasive surgery. *Biomedical Engineering, IEEE Transactions on*, 57(2):404 –414.

[Ni et al., 2011] Ni, D., Chan, W. Y., Qin, J., Chui, Y.-P., Qu, I., Ho, S., and Heng, P.-A. (2011). A virtual reality simulator for ultrasound-guided biopsy training. *Computer Graphics and Applications, IEEE*, 31(2):36 –48.

[Oddo et al., 2011] Oddo, C. M., Controzzi, M., Beccai, L., Cipriani, C., and Carrozza, M. C. (2011). Roughness encoding for discrimination of surfaces in artificial active-touch. *IEEE Trans. Robotics*, 27(3):522–533.

[Okamura et al., 2001] Okamura, A. M., Cutkosky, M. R., and I. (2001). Feature detection for haptic exploration with robotic fingers. *The International Journal of Robotics Research*, 20(12):925–938.

[Scilingo, 2010] Scilingo, E.P.; Bianchi, M. G. G. B. A. (2010). Rendering softness- integration of kinesthetic and cutaneous information in a haptic device. *IEEE Transactions on Haptics*, 3:109 – 118.

[Srinivasan and LaMotte, 1995] Srinivasan, M. A. and LaMotte, R. H. (1995). Tactual discrimination of softness: Abilities and mechanisms. *J Neurophysiol*, 73:88–101.

[Tiest, 2010] Tiest, W. M. B. (2010). Tactual perception of material properties. *Vision Research*, 50(24):2775 – 2782. Perception and Action: Part I.

[van Kuilenburg et al., 2013] van Kuilenburg, J., Masen, M. A., and van der Heide, E. (2013). A review of fingerpad contact mechanics and friction and how this affects tactile perception. *Proceedings of the Institution of Mechanical Engineers, Part J: Journal of Engineering Tribology*.

[Xu et al., 2013] Xu, D., Loeb, G. E., and Fishel, J. A. (2013). Tactile identification of objects using bayesian exploration. In *ICRA 2013*.